Effect of Clay and Mineralogy on Permeability

José M. Carcione,[1,2] Davide Gei,[1] Ting Yu,[2] and Jing Ba[2]

Abstract—The absolute permeability of rock depends on several factors, including porosity, ϕ, the geometry of the pore network (tortuosity), and the grain geometry, dimension and composition. The mineralogical composition plays an important role, mostly with respect to clay, which involves several components including illite, smectite, kaolinite and chlorite. The presence of quartz and feldspar increases permeability, while clay minerals and calcite tend to have the opposite effect. Essentially, permeability decreases with a smaller grain radius, increasing tortuosity of the pore space and decreasing porosity. As the specific surface area of the pores increases, permeability decreases. Here, we compare four expressions for permeability based on clay content, grain dimension, tortuosity and mineral composition. All the expressions somehow contain the Kozeny–Carman (KC) factor $\phi^3/(1-\phi)^2$, which is obtained on physical grounds, and relies on fitting parameters related to the geometric characteristics of the rock and its composition. The Herron model is based on geochemical mineralogy composition. Despite the highly idealized parameters on which these models are based, the results support the predictive power of the Kozeny–Carman equation, provided that proper calibration is performed.

Key words: Permeability, Kozeny–Carman factor, clay content, grain size, tortuosity, mineralogy.

1. Introduction

Permeability is important in groundwater flow (Neuzil 1994), hydrocarbon production and CO_2 storage. Over the past 30 years, the success of CO_2 storage has relied on a good estimation of permeability in the reservoir and particularly on the seal caprock and overburden to avoid possible leakage (Savioli et al. 2016). Low permeability is required in this case, which strongly depends on clay content and mineralogy. Permeability is also a key factor in levee breach flood disasters, since levees in a river may collapse due to the condition of the soils (high-permeability zones) that form the embankments (Sinha et al. 2017).

Fine-grained sediments, mud and its lithified versions (mudstone and shale), form approximately 70% of the sedimentary basins. The permeability of shales is several orders of magnitude lower than that of coarser-grained rocks such as sandstone. Therefore, shales and even sandstones with a moderate amount of clay content (shaly sandstones) control the flow at which fluids move underground. Clay can reduce porosity, increase tortuosity and block the pore throats.

The determination of clay content, defined here as the volume fraction of particles less than 4 μm in diameter, is required to obtain reliable values of permeability, since this is strongly correlated with the grain and pore size distributions. To describe permeability, we use Kozeny–Carman type equations (Kozeny 1927; Carman 1961; Tiab and Donaldson 2012) based on grain size, tortuosity and clay content, which implicitly involves several minerals, including kaolinite, illite and smectite. Herron (1987) used explicit mineralogical information available from geochemistry to obtain estimates of both porosity and permeability. He quantified the effects of the minerals comprising the rock by defining specific weights. These are positive for quartz and feldspar, negative for cements such as calcite or other carbonates, and negative for the clay minerals. The permeability logs obtained by Herron show good agreement with air permeability measured on core samples. Recently, Ma (2015) reviewed permeability models, other than the Kozeny–Carman equations, based on the power law and the exponential and polynomial dependence of porosity. Al Ismail and Zoback (2016) investigated

[1] Istituto Nazionale di Oceanografia e di Geofisica Sperimentale (OGS), Borgo Grotta Gigante 42c, 34010 Sgonico, Trieste, Italy.

[2] School of Earth Sciences and Engineering, Hohai University, Nanjing 211100, China. E-mail: jba@hhu.edu.cn

the effect of mineralogy in experiments on organic shale samples, considering mainly clay and calcite (illite was the predominant clay mineral). The authors found that shale mineralogy did not show a clear effect on the magnitude of permeability. However, caution is required when interpreting permeability based on the Kozeny–Carman equation, since there is no one-to-one relation between porosity and permeability, because porosity is invariant under a homothetic transformation of the pore space (e.g., uniform, isotropic stretching), whereas permeability is not (Bernabé et al. 2003).

One important effect to consider when using permeability models is that permeability obtained with gas may yield higher values than that based on liquids. The difference between gas and fluid permeability is due to the Klinkenberg effect (e.g., Tanikawa and Shimamoto 2006). This effect is important at low pressures and is due to the slip flow of gas at pore walls, which enhances the gas flow, especially when the pore sizes are very small; thus it can be important in shales. In this case, the physical laws leading to the Kozeny–Carman (KC) equation do not hold, and a correction must be applied.

Here, we consider four models of permeability, which are generalizations of the Kozeny–Carman equation that incorporate clay content. The grain radii and tortuosity, in addition to the KC porosity factor, are the parameters for three of these models, whereas the fourth equation is based on mineralogy (Herron 1987). Comparisons among these models and with experimental data sets are carried out in order to assess the performance of the permeability expressions.

2. Permeability Based on Grain Radii and Tortuosity

Permeability can be described by the Kozeny–Carman equation (see Appendix 1, where a demonstration is given). In this section, we present three different models, based on grain radii, tortuosity and specific surface area. We assume that the radius of the sand particles is much greater than the radius of the clay particles, by at least a factor of 5.

2.1. Model 1

A simple model introduced by Carcione et al. (2000) assumes that a medium composed of clay and sand grains of single porosity ϕ and clay content C has the partial permeability values given in Eq. (43) (Appendix 2). There is permeability anisotropy, with the vertical component dominating the flow. The permeability components are determined by an analogy with a parallel and series connections of electrical resistance (horizontal and vertical component, respectively), as shown in Fig. 1a, b, respectively, assuming that permeability is analogous to the inverse of the electrical resistance. Similarly, this distinction between horizontal and vertical permeability can be obtained from an analogy with the Backus average of the shear moduli parallel and perpendicular to layering (Backus 1962; Carcione 2014).

The horizontal component is given by $\kappa_h = (1 - C)\kappa_s + C\kappa_c$, which from Eqs. (40) and (43) does not depend on the clay content and is equal to the $C = 0$ curve (regardless of the amount of clay, the fluid will flow through the less resistant element of the parallel connection, i.e., mainly through the sand component). This assumption is too strong and can give unrealistic values of the permeability anisotropy for $r_s \gg r_c$, where r_s and r_c are the radii of the sand and clay particles, respectively. A suitable model assumes that the sandy part is affected by a given fraction of clay, say, α. Then, according to
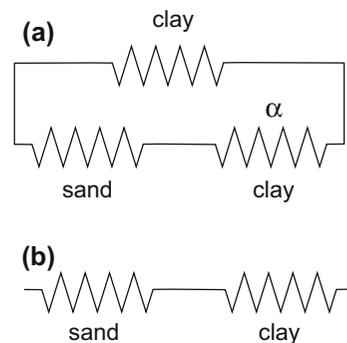

Figure 1
Electrical circuit analogy to obtain the horizontal (**a**) and vertical (**b**) permeability components. In (**a**) the sandy part is affected by a clay fraction αC

the electrical circuit shown in Fig. 1a, the horizontal component is given by

$$\kappa_h = (1 - C)\left(\frac{1 - \alpha C}{\kappa_s} + \frac{\alpha C}{\kappa_c}\right)^{-1} + C\kappa_c. \quad (1)$$

A value of $\alpha = 0.2$ yields anisotropy levels in agreement with experimental data if $r_s = 50$ μm and $r_c = 1$ μm (Clennell et al. 1999; Adams et al. 2016).

On the other hand, the average (inverse) vertical permeability of the composite medium satisfies

$$\frac{1}{\kappa_v} = \frac{1 - C}{\kappa_s} + \frac{C}{\kappa_c} = \frac{(1 - \phi)^2}{a\phi^3}\left[(1 - C)^2 + C^2 b^2\right], \quad (2)$$

where $a = r_s^2/45$ and $b = r_s/r_c$, but in practice they are used as free parameters obtained from calibration of available data. These parameters contain information about the geometric characteristics of the rock frame, such as the mean radius of the grains and the effective tortuosity $\mathcal{T}$ of the sand/clay frame network. Actually, the factor 45 has been obtained in Appendix 2 as 18 $\mathcal{T}$, with $\mathcal{T} = 2.5$, which is an idealization for spherical grains, but one cannot expect to fit real data by considering a and b a result of such an ideal assumption.

2.2. Model 2

The more commonly used model of permeability is usually given in terms of tortuosity,

$$\kappa = \frac{r_g^2 \phi^3}{18\mathcal{T}(1 - \phi)^2}, \quad (3)$$

(see demonstration in Appendix 1), where

$$r_g^{-1} = Cr_c^{-1} + (1 - C)r_s^{-1}, \quad (4)$$

is the average grain radius (Dullien 1991), and $\mathcal{T}$ is the tortuosity defined in Eq. (28) and given by Eqs. (34) and (37) for specific topologies of the pore space, namely, 3D interpenetrating tubes and solid particles flowing in a fluid, respectively. Equation (4) assumes that the densities of the sand and clay particles are the same.

2.3. Model 3

A well-known model for obtaining the permeability of sand/clay mixtures is that of Marion (1990), which considers that the two rock components each have their own porosity, ϕ_s and ϕ_c, specific surface area, s_s and s_c, and tortuosity, $\mathcal{T}_s$ and $\mathcal{T}_c$, respectively, for sand and clay. In sandstone and shaly sandstone, the clay minerals are located within the sand pore space, while for shale and sandy shale, clay is the frame and the sand grains are dispersed.

The expressions for permeability are based on Eqs. (31), (32) and (37) of Appendix 1, corresponding to the specific surface area, permeability and tortuosity, respectively. We have (Marion 1990),

$$\kappa = \frac{\phi^3}{2s^2\mathcal{T}}, \quad (5)$$

where

$$\phi = \begin{cases} \phi_s - C(1 - \phi_c), & C \leq \phi_s, \\ C\phi_c, & C > \phi_s, \end{cases} \quad (6)$$

$$s = \begin{cases} s_s + Cs_c, & C \leq \phi_s, \\ s_s\frac{1-C}{1-\phi_s} + Cs_c, & C > \phi_s, \end{cases} \quad (7)$$

$$\mathcal{T} = \begin{cases} \mathcal{T}_s\left[1 + \frac{C}{\phi_s}(\mathcal{T}_c - 1)\right], & C \leq \phi_s, \\ \mathcal{T}_c\left[1 + \frac{\mathcal{T}_s - 1}{\phi_s - 1}(C - 1)\right], & C > \phi_s, \end{cases} \quad (8)$$

where

$$s_s = \frac{3(1 - \phi_s)}{r_s}, \quad s_c = \frac{3(1 - \phi_c)}{r_c}, \quad (9)$$

and

$$\mathcal{T}_s = 1 - 0.5\left(1 - \frac{1}{\phi_s}\right), \quad \mathcal{T}_c = 1 - 0.5\left(1 - \frac{1}{\phi_c}\right). \quad (10)$$

Actually, Marion (1990) gives the equation $\kappa = \phi^3/(k_0\mathcal{T}^2s^2)$, where $\mathcal{T} = l/L$ is the square root of the tortuosity defined in the present work [see Eq. (28) in Appendix 1] and k_0 is an empirical constant. Basically, apart from the clay content C, the free parameters are r_s, r_c, ϕ_s and ϕ_c. If we assume $\phi_s = \phi_c$, we have the same number of free parameters as model 1, i.e., the radii of the sand and clay particles. In this case,

$$\phi_{\rm s} = \begin{cases} \frac{\phi+C}{1+C}, & C \le \phi_{\rm s}, \\ \phi/C, & C > \phi_{\rm s}. \end{cases} \quad (11)$$

Note this limitation of Eq. (10): the porosity, and therefore the tortuosity, is grain-size-independent for an ordered packing of identical spheres, but this is not true for a random arrangement of spheres, which is the case for rocks.

Another approach for obtaining permeability (not used here) is based on specific surface area s, if available from laboratory measurements. In this case, one can avoid using the clay content. The permeability is given by Eq. (31). Surface areas, $s_{\rm m}$, are usually given in m^2/g (mass normalized) (see Kuila and Prasad 2013). The volume-normalized surface area is then $s = s_{\rm m}\rho$, where ρ is the density of the rock.

2.4. Model 4

The Kozeny–Carman equation is based on ideal geometries of the pore space and solid component. This is clear in the demonstration given in Appendix 1, when we obtain the specific surface area. The fact that grains are non-spherical and non-uniform in size and that the grain packing is non-uniform is not considered. These issues are all directly or indirectly related to mineral composition, and it therefore makes sense that a combination of porosity and mineral abundance would lead to an improved permeability estimation.

Clay particles (smectite, kaolinite, montmorillonite, illite, chlorite, etc.) are much smaller in size than silt particles, even though all soils with particles less than 60 μm are classified as either silt or clay; specifically, the silt grain diameter ranges from 4 to 60 μm, and clay less than 4 μm. Feldspars have diameters similar to those of silt particles (Stevens 1991).

The Herron model (Herron 1987) takes into account the mineralogical composition instead of the radii of the particles. The permeability is given by

$$\log_{10}[\kappa(\text{mdarcy})] = A + 3\log_{10}\phi - 2\log_{10}(1-\phi) + \sum_i B'_i M_i, \quad (12)$$

or

$$\kappa = \frac{\phi^3}{(1-\phi)^2} 10^{A+\sum_i B'_i M_i}, \quad (13)$$

where M_i is the weight fraction of each mineral and B'_i is a constant for each mineral, related somehow to the radii of the particles,

$$A = A_0 + 2F_{\max}, \quad (14)$$

where A_0 is a constant and $F_{\max}$ is the maximum feldspar content. The coefficients used by Herron (1987) are as follows:

Quartz: $B'_1 = 0.1$
Feldspar: $B'_2 = 1$
Calcite: $B'_3 = -2.5$
Kaolinite: $B'_4 = -4.5$
Illite: $B'_5 = -5.5$
Smectite: $B'_6 = -7.5$

The quantity $A_0 = 4.9$ for the area considered by Herron (1987) (Venezuela, Faja del Orinoco region), but it has to be calibrated for the specific region. It is a function of the maximum feldspar content in a given zone, which reflects the compositional and textural maturity of the sediment. Herron (1987) estimated A_0 and B'_i from comparisons between air permeability measurements on cores and mineralogy abundance values derived from geochemical logging in the same wells.

Note that Eq. (14) is a Kozeny–Carman equation, since basically

$$\kappa \propto \frac{\phi^3}{(1-\phi)^2}.$$

2.5. Modified Models Including Percolation Porosity

There exists a percolation porosity, $\phi_{\rm c}$, below which the porosity is disconnected and does not contribute to the flow. The experiments indicate that $\phi_{\rm c}$ is of the order of 1–3% (Porter et al. 2013). The percolation effect can be incorporated into the Kozeny–Carman relations simply by replacing ϕ with $\phi - \phi_{\rm c}$. For instance, model (2) is modified as

$$\frac{1}{\kappa} = \frac{(1-\phi+\phi_{\rm c})^2}{a(\phi-\phi_{\rm c})^3}\left[(1-C)^2 + C^2 b^2\right]. \quad (15)$$

2.6. Results

Figures 2 and 3 show comparisons between model 1 (vertical permeability) and models 2 and 3, respectively. Model 3 assumes that $\phi_s = \phi_c$ [Eq. (11)]. In the first case, the curves are very similar and differ only at low porosities. As porosity increases, permeability increases, as expected. Small amounts of clay content greatly affect the permeability. For instance, going from $C = 0$ to $C = 0.2$ implies a two-orders-of magnitude change, from 1 to 10 mdarcy for $\phi = 0.4$. On the other hand, the permeability of model 3 differs substantially from that of the other models. Essentially, the permeability of the Marion model has negligible variation when the clay content is higher than 0.4, providing higher permeability values than the other models.
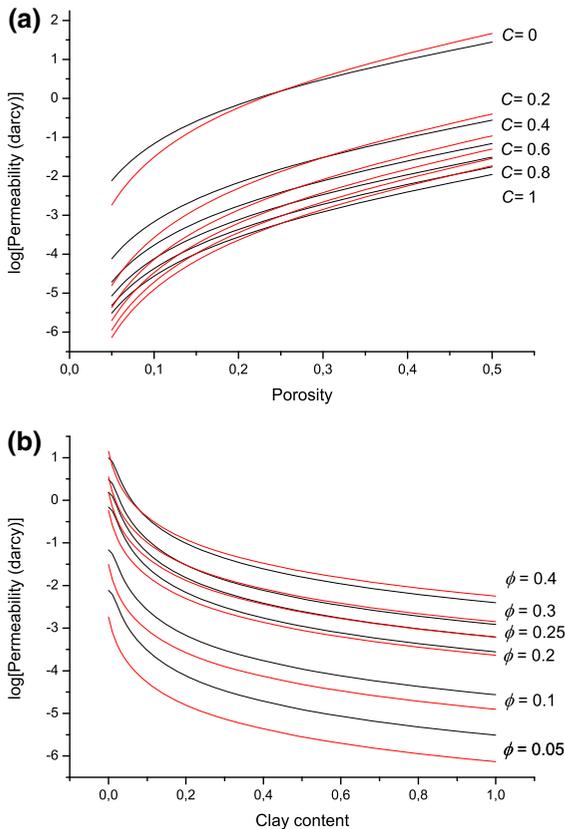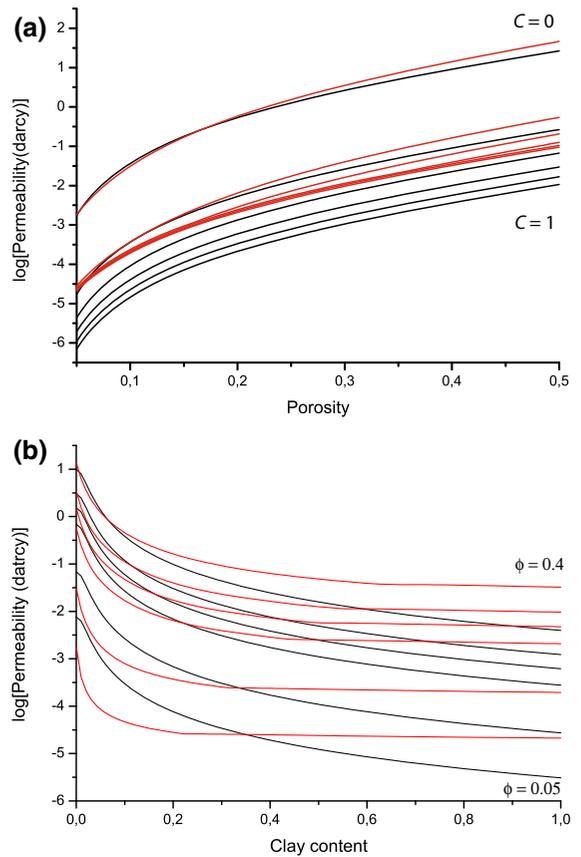

Figure 2

Permeability versus porosity (**a**) and clay content (**b**) for different values of clay content and porosity, respectively. The black and red lines correspond to Eqs. (2) and (3), respectively (models 1 and 2). The radii of the sand and clay particles are $r_s = 50$ μm and $r_c = 1$ μm, respectively

Figure 3

Permeability versus porosity (**a**) and clay content (**b**) for different values of clay content and porosity, respectively. The black and red lines correspond to Eqs. (2) and (5), respectively (models 1 and 3). The radii of the sand and clay particles are $r_s = 50$ μm and $r_c = 1$ μm, respectively

Next, we consider 13 Gulf Coast shaly sandstone samples (Marion 1990) and compare these data with the results for models 1 and 3. The data are permeability as a function of clay content by weight, C_w. The relation to clay (volume) content, C, is (Marion 1990)

$$C_w = \begin{cases} \dfrac{C(1-\phi_c)\rho_c}{C(1-\phi_c)\rho_c+(1-\phi_s)\rho_s}, & C \le \phi_s, \\ \dfrac{C(1-\phi_c)\rho_c}{C(1-\phi_c)\rho_c+(1-C)\rho_s}, & C > \phi_s, \end{cases} \qquad (16)$$

where ρ_s and ρ_c are the density of the sand and clay grains, respectively. Inverting for C:

$$C = \begin{cases} \dfrac{C_w(1-\phi_s)\rho_s}{(1-C_w)(1-\phi_c)\rho_c}, & C \le \phi_s, \\ \dfrac{C_w\rho_s}{(1-\phi_c)\rho_c-C_w[(1-\phi_c)\rho_c-\rho_s]}, & C > \phi_s. \end{cases} \qquad (17)$$

We consider the values given in Table 3.2 of Marion (1990), i.e, ρ_s = 2.568 g/cm^3, ρ_c = 2.77 g/cm^3, ϕ_s = 0.32, ϕ_c = 0.25, $\mathcal{T}_s$ = 1.5 and $\mathcal{T}_c$ = 10. Marion (1990) takes the specific surface area as a free parameter, but here we use Eq. (9), i.e., the radii. Also, the additional free parameter k_0 in eq. (3.14) of Marion (1990) (not reported) is not used here. For the sake of consistency, the porosity and clay content obtained from model 3 are used for model 1. Figure 4 shows the permeability as a function of clay content, where the black and red lines correspond to Eqs. (5) and (2), respectively. As can be seen, the two models yield similar results.

A fit of experimental data reported in Chilingar (1969) is shown in Fig. 5 for different mineral composition from very coarse sand to clay. The radii of the sand and clay particles are r_s = 150 μm and r_c = 5 μm, respectively. The agreement is satisfactory. Finally, to illustrate the effects of percolation porosity, Fig. 6 shows the results corresponding to Fig. 2 with ϕ_c = 0.02. As can be appreciated, the curves move to the lower permeability values.

Nelson (1994) used the Herron model to obtain permeability versus porosity and clay content. His Fig. 21 is reproduced here in Fig. 7, noting that the A values are not reported in Nelson (1994) (here we take $F_{max} = M_2$) and that the B values used by Nelson
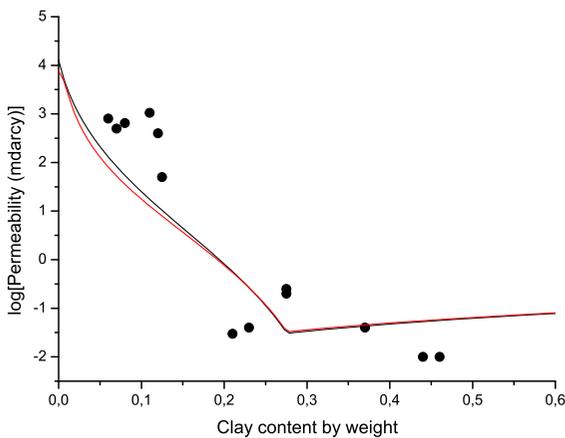

Figure 4

Permeability versus clay content. The black and red lines correspond to Eqs. (5) (model 3) and (2) (model 1), respectively, and the dots to the experimental data (Marion 1990). The radii of the sand and clay particles are r_s = 70 μm and r_c = 1 μm in the first case (model 3), and r_s = 70 μm and r_c = 0.5 μm in the second case (model 1), respectively

in his eq. (8) are not the same of those reported in his Fig. 21, which should be B' [see Herron (1987), his eqs. (4) and (5)]. The equivalence is given by $\log_{10}[\exp(\sum B_i M_i)] = \sum B'_i M_i$ or $B_i = 2.3026 B'_i$. Figure 7 also shows a curve (dotted line) obtained with our Eq. (2) for case 4, where C = 0.16 (kaolinite), using r_s = 50 μm and r_c = 5 μm. This curve coincides with that of case 4. To obtain it, we have converted weight fraction to volume fraction using the equations in Appendix 3. The densities of the different minerals are as follows: ρ_s = 2.65 g/cm^3, ρ_{fp} = 2.62 g/cm^3, ρ_c = 2.71 g/cm^3, ρ_k = 1.58 g/cm^3, ρ_{il} = 2.7 g/cm^3, ρ_{sm} = 2.4 g/cm^3, ρ_{ch} = 2.8 g/cm^3, for quartz, feldspar, calcite, kaolinite, illite, smectite and chlorite, respectively.

Herron B'_i values are not universal, and calibration is required for each area. The following is an example: Let us consider the experimental values of Fig. 5 in Mesri and Olson (1971), which represent the void ratio, e, as a function of the hydraulic permeability, K, for three sodium clays in water, i.e., smectite, illite and kaolinite. Illite is about 200 times more pervious than smectite, and kaolinite is about 200,000 times more pervious, at the same void ratio. Porosity and void ratio are related as $\phi = e/(1 + e)$, while the absolute permeability is

$$\kappa = \frac{\eta_w K}{g \rho_w},$$

where η_w = 0.001 Pa s is the viscosity of water, ρ_w = 1000 kg/m^3 is water density, and g = 9.86 m/s^2 is the gravity constant. We use Eq. (12) for each clay, in the form

$$\log_{10}[\kappa(\text{mdarcy})] = A + 3\log_{10}\phi - 2\log_{10}(1 - \phi) + B',$$

(18)

where B' is the Herron coefficient. Figure 8 shows the match between the experimental values and the results of Eq. (18) with A = 4.3, B' = − 7.5 (smectite), B' = − 5.5 (illite), and B' = − 3 (kaolinite), which are quite similar to Herron values.

In the following examples, we adopt Herron B' values. Next, we consider ten wells whose data are given in Tables 1 and 2 of Liu et al. (2016), where the illite/smectite mixed layer has been decomposed into illite and smectite. Permeability has been
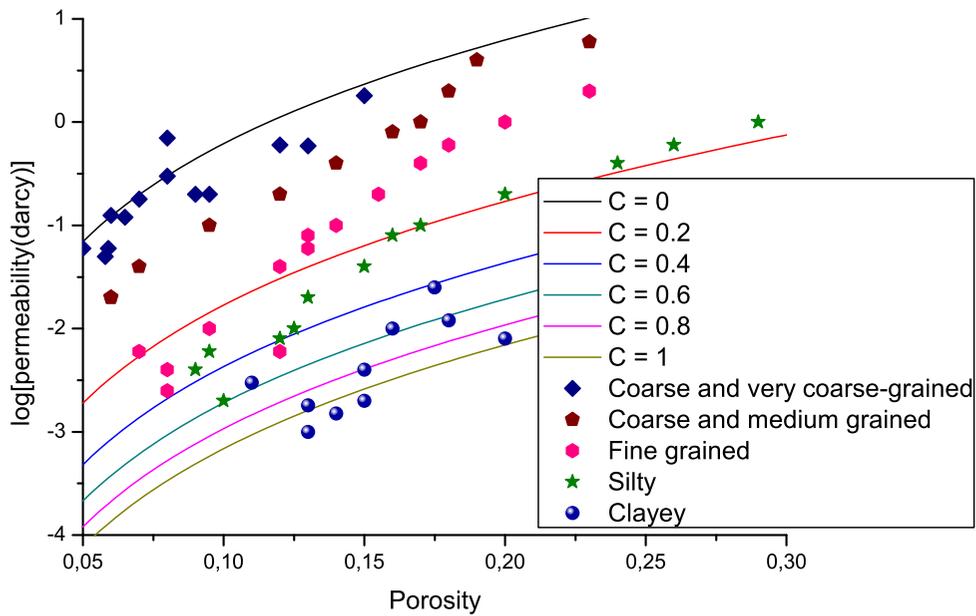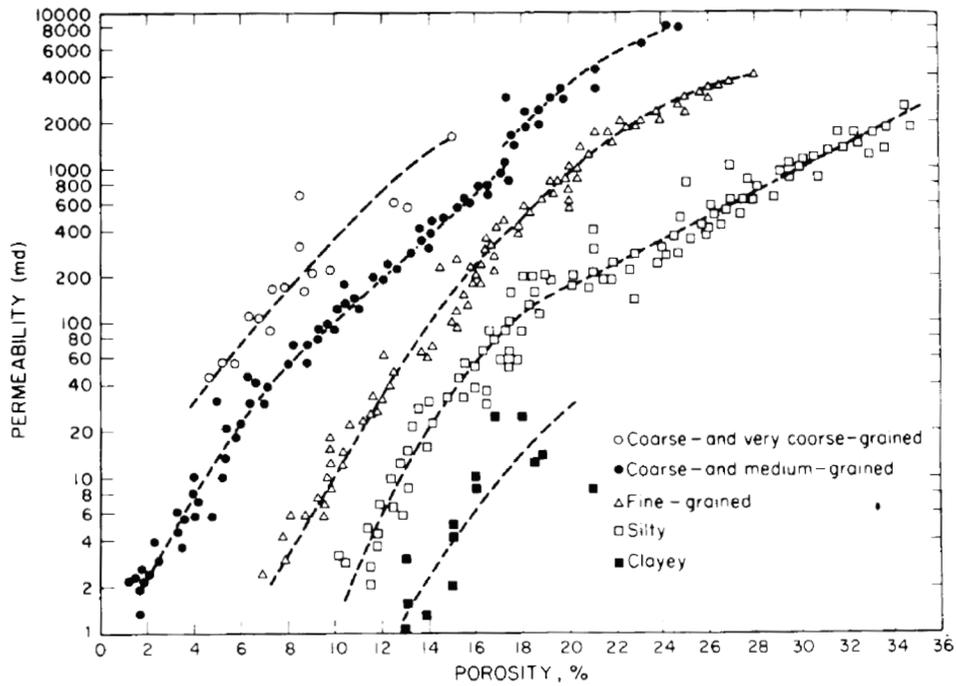
Figure 5
Comparison with experimental data (Chilingar [1969]) using Eq. (2) (model 1). The radii of the sand and clay particles are $r_s = 150$ μm and $r_c = 5$ μm, respectively

measured with water. Plagioclase is a series of tectosilicate (framework silicate) minerals within the feldspar group, so we included this mineral in

the feldspar composition. Table 1 here shows the mineral composition, porosity and permeability at the ten wells. We take $A_0 = 3.5$, F_{max} = feldspar weight
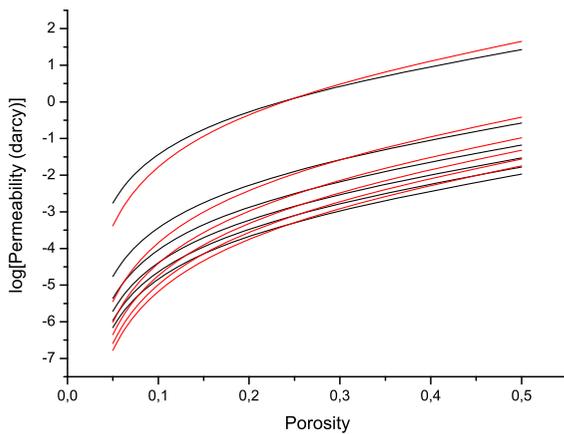
Figure 6

Permeability versus porosity for different values of clay content. The black and red lines correspond to Eqs. (2) and (3), respectively (models 1 and 2). The radii of the sand and clay particles are r_s = 50 μm and r_c = 1 μm, respectively. These curves are affected by a percolation porosity ϕ_c = 0.02 (compare to Fig. 1, where the percolation porosity is zero)
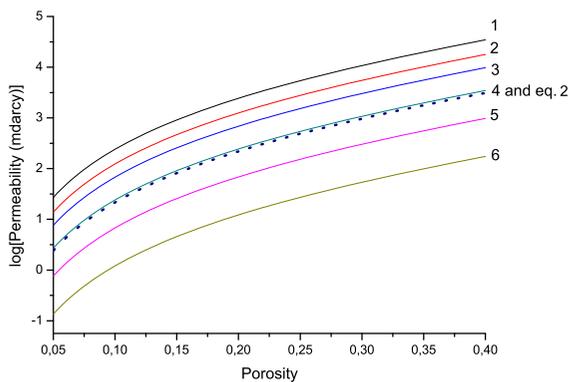

Figure 7

Permeability versus porosity for different mineralogical composition, using Eq. (12) (model 4). The six cases are as follows: case 1: M_1 = 0.9 and M_2 = 0.1; case 2: M_1 = 1; case 3: M_1 = 0.9 and M_3 = 0.1; case 4: M_1 = 0.9 and M_4 = 0.1; case 5: M_1 = 0.9 and M_5 = 0.1; case 6: M_1 = 0.9 and M_6 = 0.1. The dotted curve obtained from Eq. (2) (model 1) coincides with that of case 4. The radii of the sand and clay particles in Eq. (2) are r_s = 50 μm and r_c = 5 μm, respectively

percent (see Table 1) divided by 100 and assume that chlorite has a coefficient B'_7 = − 6. Figure 9 compares the experimental data to the model results, where it can be seen that the match with the Herron model is satisfactory. The blue curve corresponds to Eq. (2), where we have converted weight fractions to volume fractions and assumed that clay content is given by the sum of the kaolinite, illite, smectite and
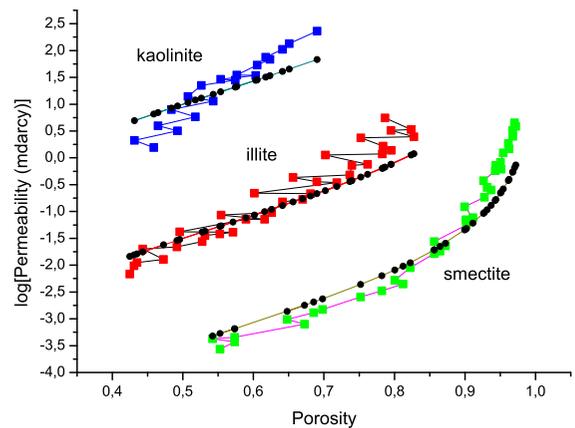

Figure 8

Comparison between experimental data (square symbols, from Mesri and Olson 1971) and the results of the Herron model (model 4) [solid circles, Eq. (18)] for three clays

chlorite fractions. In this case, r_s = 50 μm and r_c = 0.9 μm.

Klimentos and McCann (1990) provide a complete set of petrographic data for a shaly sandstone (their Table 2, rock sample A6BP), where we consider the X-ray diffraction values. Porosity is 15.4%, permeability is 52.4 mdarcy, the average (clastic) grain size is 330 μm, and the clay grain size is less than 2 μm. The volume fractions are quartz 53%, feldspar 32%, kaolinite 13.5% and illite 1.5%, so that the clay content is C = 15% (kaolinite plus illite). On the basis of the mineral densities indicated above, the weight fractions are M_1 = 56.2%, M_2 = 33.6%, M_4 = 8.5% and M_5 = 1.7%. Model 1 provides a perfect fit with r_s = 330 μm and r_c = 3.2 μm, which are reasonable values given the highly idealized assumptions. On the other hand, the Herron model yields a perfect fit with A_0 = 3.42.

Finally, we consider the data of Backeberg et al. (2017). Table 2 shows the composition of samples #2 and #4 given in their Table 1, together with the porosity, permeability and Herron coefficients B'. The reported permeability was measured with water; surprisingly, the authors obtained a lower value for argon permeability, in contrast to the Klinkenberg effect (e.g., Tanikawa and Shimamoto 2006). In order to use the Herron equation (12), the volume composition must be converted to solid volume composition and then to weight composition using Eq. (48). The B' values of quartz, calcite, illite, kaolinite and

Table 1

Mineral composite, porosity and permeability for ten wells of the Zhenbei area (China) (Liu et al. 2016)

Well	Quartz	Feldspar	Calcite	Kaolinite	Illite	Smectite	Chlorite	ϕ	κ
Z-1	36	20	25	2.47	7	0.98	8.55	10.23	0.385
Z-2	38	22	18	1.8	10	1.61	8.58	7.84	0.184
Z-3	43	20	17	2.8	8	0.6	8.6	9.13	0.327
Z-4	30	23	22	1.5	14	2.75	6.75	6.637	0.121
Z-5	42	24	12	2.2	10.2	1.9	7.7	7.06	0.149
Z-6	45	21	13	2.31	10	1.8	6.9	8.46	0.251
Z-7	36	23	18	2	11.9	1.28	7.82	8.06	0.214
Z-8	42	19	20	3	7	1.4	7.6	9.85	0.352
Z-9	36	25	15	0.5	14.1	2.7	6.72	6.837	0.132
Z-10	40	20	17	3.2	10.3	1.7	7.8	7.11	0.163

Mineral composition [weight%]; porosity [volume%]; κ [mdarcy]

Table 2

Mineral composition (volume%) and properties (Backeberg et al. 2017)

Sample	#2	#4	ρ (g/cm^3)	B'
Quartz	11.2	9.6	2.65	0.1
Plagioclase	2.9	3.6	2.62	1
Dolomite	2.9	9.6	2.9	$-$ 2.5
Calcite	0.6	1.3	2.71	$-$ 2.5
Muscovite	6.3	5.6	2.81	1
Pyrite	1.3	1.6	4.8	$-$ 2.5
Trace minerals	11	4	2.6	$-$ 2.5
Porous space	1.5	3.4	1.7	$-$
Illite	49.8	49	2.7	$-$ 5.5
Kaolinite	8.7	8.6	1.58	$-$ 4.5
Smectite	3.8	3.7	2.4	$-$ 7.5
ϕ (volume%)	1.5	3.4	$-$	$-$
κ (mdarcy)	0.35	0.4	$-$	$-$

smectite in Table 2 are taken from Herron (1987). Plagioclase and muscovite are treated as feldspar, and dolomite, pyrite and trace minerals as calcite, since they tend to block the flow. The organic matter [kerogen as reported by Backeberg et al. (2017)] is part of the pore space, which was obtained with the QEMSCAN measurement (Quantitative Evaluation of Minerals by SCANning electron microscopy), to be consistent with the reported volume composition. With the values given in Table 2, we can obtain a perfect fit of the experimental permeability values with Eqs. (2) and (12), by setting for sample #2: $r_s = 50$ μm, $r_c = 0.044$ μm, $A_0 = 2.65$, $F_{max} = 0.0862$; sample #4: $r_s = 50$ μm, $r_c = 0.014$ μm, $A_0 = 1.68$,

$F_{max} = 0.0891$, where F_{max} is the feldspar proportion given by the sum of the plagioclase and muscovite proportions. Clay content for Eq. (2) is the sum of the illite, kaolinite and smectite proportions, after proper normalization. Bulk densities of 2.52 g/cm^3 and 2.53 g/cm^3 are obtained, against the measured values of 2.52 g/cm^3 and 2.6 g/cm^3, respectively, for samples #2 and #4. Figure 10 shows a fit by assuming a common value $r_c = 0.02$ μm for model 1 and $A_0 = 2$ for the Herron model. The two models yield the same result.

Another technique introduced by Herron et al. (1998, 2002) evaluates permeability based on the lambda parameter, which is a measure of the effective diameter of dynamically connected pores, and which can be approximated from the surface-to-pore-volume ratio. The surface-to-pore-volume ratio can be computed from mineralogy data. The other required input data are the total porosity, the matrix density and Archie's cementation exponent.

Methods based on the Kozeny–Carman equation require defined values of porosity, grain radii, surface area, etc., in order to be applied. Alternative techniques, such as neural networks, do not require these data. Regarding hydrocarbon exploration, several works using this technique have been published. Helle et al. (2001) and Qadrouh et al. (2019), for instance, have predicted porosity and permeability from wireline logs using artificial neural networks. The two techniques can be integrated to provide more reliable results.
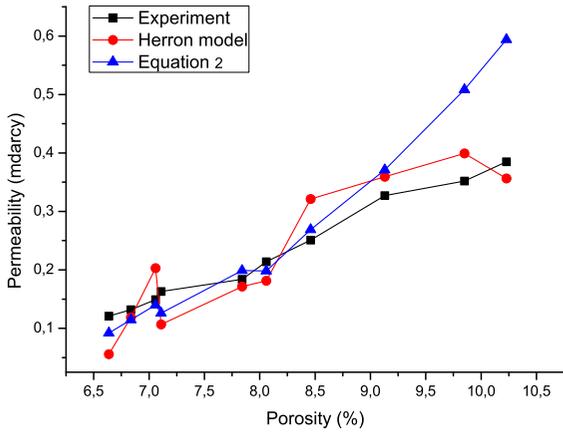
Figure 9

Comparison between experimental data (black, Liu et al. 2016), the results of the Herron model (model 4) [red, Eq. (12)] based on mineral composition, and those of Eq. (2) (blue)
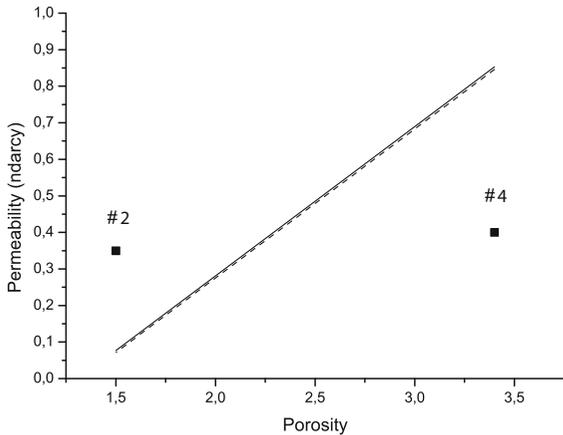

Figure 10

Comparison between experimental data (symbols) (Backeberg et al. 2017) and the results of Eqs. (2) (model 2, dashed line) and (12) (solid line, Herron, model 4). We assume that $r_c = 0.02$ μm for model 1 and $A_0 = 2$ for the Herron model

3. Conclusions

We have compared four expressions for permeability of the Kozeny–Carman family of equations, which are based on physical parameters including porosity, grain and pore size, tortuosity and mineral composition. This aspect makes this equation predictive, unlike simple polynomial fittings. The use of geochemical mineralogy represents a significant improvement in formation characterization over that of geophysical log data alone. The model to be used
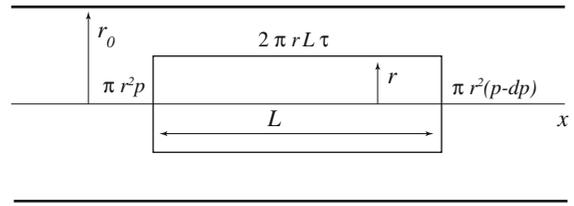

Figure 11

Initial reference model for obtaining permeability as a function of porosity. Balance of forces on a cylindrical element of fluid in a pipe

for a specific case history depends on the data for calibration. Models based on grain radii and/or surface area and clay content are the most common. If, in addition, mineral composition of clays is available, the Herron model provides a better estimation of permeability. All models can be applied to sandstones and shales and mixed composition of sand and clay. Although the geometric characteristics of the porous rock are idealized, the equations can be used, with proper calibration, to obtain reliable estimates of permeability. The examples presented here show that this estimation is possible.

Appendix 1: Demonstration of the Kozeny–Carman Equation

Let us assume a cylindrical element of Newtonian fluid of length L and radius r flowing in a pipe of radius $r_0 > r$ along the x axis (see Fig. 11). The pressure difference between the two faces is dp. The pressure p and viscous force τ balance (the element is not accelerating). The pressure acts on the surface of the faces and the viscous force acts on the lateral surface given by πr^2 and $2\pi rL$, respectively. Then, the balance is $\pi r^2 p - (p - dp)\pi r^2 - 2\pi rL\tau = 0$, or

$$\frac{dp}{L} = 2\tau r. \tag{19}$$

Since dp does not depend on r, it is $\tau \propto r$ (τ vanishes at $r = 0$).

The shear stress obeys a dashpot-like constitutive equation,

$$\tau = -\eta \partial_r v, \tag{20}$$

where v is the flow velocity, η is the fluid viscosity, r is the radial coordinate and ∂_r denotes the partial

derivative with respect to r. Since the velocity decreases from the pipe centre to zero at the pipe wall, we need to include the minus sign ($\partial_r v < 0$ gives $\tau > 0$). Combining Eqs. (19) and (20) yields $\partial_r v = -dp/(2\eta L)$, which after integration gives

$$v = -\left(\frac{dp}{4\eta L}\right)r^2 + c, \qquad (21)$$

where c is a constant. Since $v(r_0) = 0$ (the fluid is welded to the pipe at the wall), we have

$$v = v_{max}\left(1 - \frac{r^2}{r_0^2}\right), \quad v_{max} = \frac{dp\, r_0^2}{4\eta L}. \qquad (22)$$

Integration of the velocity profile on the transverse section of the pipe yields the flow rate,

$$Q = \int_0^{r_0} \pi r v(r) dr = \frac{1}{2}\pi v_{max} r_0^2 = \frac{\pi r_0^4 dp}{8\eta L}, \qquad (23)$$

where we used Eq. (22). This is the so-called Hagen–Poiseuille law.

Appendix 1.1: Permeability

If S is the cross-sectional area of a porous sample and η is the dynamic viscosity, the permeability κ obeys

$$Q = S\frac{\kappa}{\eta}\frac{dp}{L}, \qquad (24)$$

while porosity is given by

$$\phi = \frac{\pi r_0^2 L}{SL} = \frac{\pi r_0^2}{S}. \qquad (25)$$

Using this equation and comparing Eqs. (23) and (24), we obtain

$$\kappa = \frac{\phi r_0^2}{8}. \qquad (26)$$

If the pipe forms an angle θ with the x-axis and its length is l, i.e., $\sin\theta = L/l$, the porosity is

$$\phi = \frac{\pi r_0^2 l}{SL} = \frac{\pi r_0^2 \sqrt{\mathcal{T}}}{S}, \qquad (27)$$

where

$$\mathcal{T} = \left(\frac{l}{L}\right)^2 = \frac{1}{\sin^2\theta}, \qquad (28)$$

is the tortuosity. Tortuosity is also defined as l/L. The definition here is such that the resistivity formation factor F is almost proportional to $\mathcal{T}$ (Tiab and Donaldson 2012; eq. 3.21). Now, the pressure gradient becomes $dp/l = dp/(L\sqrt{\mathcal{T}})$, and it is easy to show that the permeability becomes

$$\kappa = \frac{\phi r_0^2}{8\mathcal{T}}. \qquad (29)$$

This equation can be general if r_0 is an effective pore radius and $\mathcal{T} \geq 1$ can be obtained from experiments.

The specific surface area s is defined as the area of the pore, $2\pi r_0 l$, divided by the volume of the sample, SL. Using Eq. (25), it is

$$s = \frac{2\phi}{r_0}. \qquad (30)$$

Then

$$\kappa = \frac{\phi^3}{2s^2\mathcal{T}} \qquad (31)$$

(e.g., Chillingar 1963).

Let us consider a sphere of radius r_g (grain), embedded in a cube of length $2r_g$. The porosity obeys $1 - \phi = (4/3)\pi r_g^3/V$, where $V = 8r_g^3$ is the cube volume. The surface area is $s = 4\pi r_g^2/V$, where the numerator is the pore-space area (area of the sphere). Then,

$$s = \frac{3(1-\phi)}{r_g} \qquad (32)$$

and (31) becomes

$$\kappa = \frac{r_g^2}{18\mathcal{T}}\frac{\phi^3}{(1-\phi)^2}, \qquad (33)$$

which is the Kozeny–Carman equation (Kozeny 1927; Carman 1961).

Appendix 1.2: Expressions of Tortuosity

The Kozeny equation (31) can be recast as $\kappa = c\phi^3/s^2$, where c is the Kozeny factor (Fabricius et al. 2007). For straight 3D interpenetrating tubes, the tortuosity is given by

$$\mathcal{T} = 2 + 2\cos\left[\frac{1}{3}\arccos\left(\frac{64\phi}{\pi^3} - 1\right) + \frac{4}{3}\pi\right], \quad (34)$$

(Mortensen et al. 1998), where $\mathcal{T}$ decreases from 3 to 2 as ϕ increases from 0.05 to 0.5.

A simple expression of tortuosity for grains was obtained by Berryman (1980) in the framework of Biot's theory of poroelasticity. Nelson (1988) shows that the Biot effective densities are

$$
\begin{aligned}
\rho_{11} &= (1 - \phi)\rho_s + \phi\rho_f(\mathcal{T} - 1), \\
\rho_{12} &= -\phi\rho_f(\mathcal{T} - 1), \\
\rho_{22} &= \phi\rho_f\mathcal{T},
\end{aligned}
\tag{35}
$$

where ρ_f and ρ_s are the fluid and grain densities (see also Carcione (2014) for a complete demonstration). Interpreting ρ_{11} as

$$
\rho_{11} = (1 - \phi)(\rho_s + \gamma\rho_f),
\tag{36}
$$

where $\gamma\rho_f$ is the induced mass due to the oscillations of the solid particles in the fluid (Lamb 1945), we obtain

$$
\mathcal{T} = 1 - \gamma\left(1 - \frac{1}{\phi}\right).
\tag{37}
$$

For spherical grains ($\gamma = 1/2$), $\mathcal{T}$ decreases from 10 to 1.5 as ϕ increases from 0.05 to 0.5.

Appendix 2: Sand and Clay Partial Permeability

To obtain the permeability of the composite medium (sand–clay mixture), we consider an idealized situation wherein the solid part can be modelled as a dilute concentration of sand and clay spherical particles in the fluid. This situation is realized in the high-porosity limit ($\phi \to 1$). Since the concentration is dilute, each particle can be considered independently of the others. The viscous resistance force for a single sphere of radius r moving in a flow of average velocity v and a fluid viscosity η_f obeys Stokes's law $F = 6\pi\eta_f v r$. Suppose that in a unit volume we have n_v particles of radius r_v, $v = 1$ (sand grains) or 2 (clay particles). The viscous resistance to the flow by particles of type v can then be written as

$$
F_v = 6\pi\eta_f v n_v r_v.
\tag{38}
$$

The density numbers n_v can be thought of as the total volume of the particles of type v divided by the volume of a single particle,

$$
n_v = \frac{\phi_v}{\frac{4}{3}\pi r_v^3},
\tag{39}
$$

where

$$
\phi_1 = (1 - \phi)(1 - C), \quad \text{and} \quad \phi_2 = (1 - \phi)C,
\tag{40}
$$

are the sand and clay proportions, with C the clay content.

Substitution of (39) into Eq. (38) yields

$$
F_v = \frac{9}{2}\eta_f v\phi_v r_v^{-2},
$$

or, for the Biot viscous resistance coefficient,

$$
b_v = F_v\frac{\phi^2}{v} = \frac{9}{2}\eta_f\phi^2\phi_v r_v^{-2},
\tag{41}
$$

(Biot 1962; Carcione 2014). The quantity

$$
\kappa_v = \frac{2}{9}\frac{r_v^2}{\phi_v},
\tag{42}
$$

can be thought of as a partial permeability of the matrix formed by particles of type v. Hence, $b_v = \eta_f\phi^2/\kappa_v$, as expected (Biot 1962).

Equation (42) provides an explicit expression for the resistance coefficients in the high-porosity limit. To be consistent with the Kozeny–Carman equations (33), we divide the expression for permeability by the factor $10(1 - \phi)/\phi^3$ (see Appendix 1), which corresponds to a tortuosity of 2.5. Then,

$$
\kappa_v = \frac{r_v^2\phi^3}{45\phi_v(1 - \phi)}.
\tag{43}
$$

Appendix 3: Conversion from Weight Fraction to Volume Fraction and Vice Versa

Assume n components, each of density ρ_i and weight fraction M_i. Weight fraction is defined as

$$
M_i = \frac{\rho_i v_i}{\sum_i \rho_i v_i},
\tag{44}
$$

where v_i is the volume of each component. Volume fraction is defined as

$$
V_i = \frac{v_i}{\sum_i v_i}.
\tag{45}
$$

Then, the ratio of the total volume $v = \sum_i v_i$ to the total mass $m = \sum_i \rho_i v_i$ is

$$\frac{v}{m} = \sum_i \frac{M_i}{\rho_i}. \tag{46}$$

It is straightforward to show that

$$V_i = \frac{M_i}{\rho_i} \left(\sum_i \frac{M_i}{\rho_i} \right)^{-1}, \tag{47}$$

and

$$M_i = \frac{\rho_i V_i}{\sum_i \rho_i V_i}. \tag{48}$$

Publisher's Note   Springer Nature remains neutral with regard to jurisdictional claims in published maps and institutional affiliations.

References

Adams, A., Nordquist, T. J., Germaine, J. T., & Flemings, P. B. (2016). Permeability anisotropy and resistivity anisotropy of mechanically compressed mudrocks. *Canadian Geotechnical Journal*, *53*(9), 1474–1482.

Al Ismail, M. I., & Zoback, M. D. (2016). Effects of rock mineralogy and pore structure on stress-dependent permeability of shale samples. *Philosophical Transactions. Series A, Mathematical, Physical, and Engineering Sciences*, *374*(2078), 20150428.

Backeberg, N. R., Iacoviello, F., Rittner, M., Mitchell, T. M., Jones, A. P., Day, R., et al. (2017). Quantifying the anisotropy and tortuosity of permeable pathways in clay-rich mudstones using models based on X-ray tomography. *Scientific Reports*, *7*, 14838. https://doi.org/10.1038/s41598-017-14810-1.

Backus, G. E. (1962). Long-wave elastic anisotropy produced by horizontal layering. *Journal of Geophysical Research*, *67*, 4427–4440.

Bernabé, Y. B., Mok, U., & Evan, B. (2003). Permeability-porosity relationships in rocks subjected to various evolution processes. *Pure and Applied Geophysics*, *160*, 937–960.

Berryman J.G. (1980). Confirmation of Biot's theory. *Applied Physical Letters*, *37*, 382–384.

Biot, M. A. (1962). Mechanics of deformation and acoustic propagation in porous media. *Journal of Applied Physics*, *33*, 1482–1498.

Carcione, J. M. (2014). *Wave fields in real media. Theory and numerical simulation of wave propagation in anisotropic, anelastic, porous and electromagnetic media* (3rd ed.). Amsterdam: Elsevier.

Carcione, J. M., Gurevich, B., & Cavallini, F. (2000). A generalized Biot–Gassmann model for the acoustic properties of shaley sandstones. *Geophysical Prospecting*, *48*, 539–557.

Carman, P. C. (1961). *L' écoulement des gaz á travers les milieux poreux Bibliothéque des Sciences et Techniques Nucléaires*. Paris: Presses Universitaires de France.

Chilingar, G. V. (1963). Relationship between porosity, permeability, and surface areas of sediments. *Journal of Sedimentary Research*, *33*(3), 759–765.

Chilingar, G. V. (1969). *Deltaic and shallow marine deposits*. Amsterdam: Elsevier.

Clennell, M. B., Dewhurst, D. N., Brown, K. M., & Westbrook, G. K. (1999). Permeability anisotropy of consolidated clays. *Geological Society, London, Special Publications*, *158*, 79–96.

Dullien, F. A. L. (1991). One and two phase flow in porous media and pore structure. In D. Bideau & J. Dodds (Eds.), *Physics of granular media* (pp. 173–214). New York: Nova Science Publishers Inc.

Fabricius, I. L., Baechle, G., Eberli, G. P., & Weger, (2007). Estimating permeability of carbonate rocks from porosity and v_P/v_S. *Geophysics*, *72*, E185–E191.

Helle, H. B., Bhatt, A., & Ursin, B. (2001). Porosity and permeability prediction from wireline logs using artificial neural networks. *Geophysical Prospecting*, *49*, 431–444.

Herron M. M. (1987). *Estimating the intrinsic permeability of clastic sediments from geochemical data*. In Transactions of the SPWLA 28 the annual logging symposium, London 1987, UK, paper HH.

Herron, M. M., Johnson, D. L., & Schwartz, L. M. (1998). *A robust permeability estimator for siliciclastics*. In Paper SPE 49301 presented at the 1998 SPE annual technical conference and exhibition, New Orleans 1998, 27–30 September.

Herron, M. M., Herron, S. L., Grau, J. A., Seleznev, N. V., Philips, J., El Sherif, A., Farag, S., Horkowitz, J. P., Neville, T. J., & Kai, H. (2002). Real-time petrophysical analysis in siliciclastics from the integration of spectroscopy and triple-combo logging. In Proc. SPE Ann. technical conference and exhibition, 29 September–2 October 2002, San Antonio, USA, Society of Petroleum Engineers. https://doi.org/10.2118/77631-MS.

Klimentos, T., & McCann, C. (1990). Relationships between compressional wave attenuation, porosity, clay content, and permeability of sandstones. *Geophysics*, *55*, 998–1014.

Kozeny, J. (1927). Über kapillare leitung des Wassers im Boden. *Sitzungsberichte der Wiener Akademie des Wissenschaften*, *136*, 271–306.

Kuila, U., & Prasad, M. (2013). Specific surface area and pore-size distribution in clays and shales. *Geophysical Prospecting*, *61*, 341–362.

Lamb, H. (1945). *Hydrodynamics* (pp. 152–156). New York: Dover.

Liu, G., Li, S., Gu, D., Lu, Y., & Asamoah, E. (2016). Experimental study of petrophysical properties of a tight formation by considering the clay minerals and flow sensitivities. *Earth Sciences Research Journal*, *20*, B1–B6.

Ma, J. (2015). Review of permeability evolution model for fractured porous media. *Journal of Rock Mechanics and Geotechnical Engineering*, *7*, 351–357.

Marion, D. (1990). *Acoustical, mechanical and transport properties of sediments and granular materials*. Stanford: Stanford University.

Mesri, G., & Olson, R. E. (1971). Mechanisms controlling the permeability of clays. *Clays and Clay Minerals*, *19*, 151–158.

Mortensen, J., Engstrøm, F., & Lind, I. (1998). The relation among porosity, permeability, and specific surface of chalk from the

Gorm field, Danish North Sea. *SPE Reservoir Evaluation & Engineering*, *1*, 245–251.

Nelson, J. T. (1988). *Acoustic emission in a fluid saturated heterogeneous porous layer with application to hydraulic fracture*. California: University of California. **(PhD thesis)**.

Nelson, P. (1994). Permeability-porosity relationships in sedimentary rocks. *The Log Analyst*, *35*(3), 38–62.

Neuzil, C. E. (1994). How permeable are clays and shales? *Water Resources Research*, *30*(2), 145–150.

Porter, L. B., Ritzi, R. W., Mastera, L. J., Dominic, D. F., & Ghanbarian-Alavijeh, B. (2013). The Kozeny–Carman equation with a percolation threshold. *Ground Water*, *51*, 92–99.

Qadrouh, A. N., Carcione, J. M., Alajmi, M., & Alyousif, M. M. (2019). A tutorial on machine learning with geophysical applications. *Bollettino Geofisica Teorica E Applicata*. **(submitted)**

Stevens, R. L. (1991). Grain-size distribution of quartz and feldspar extracts and implications for flocculation processes. *Geo-marine Letters*, *11*, 162–165.

Savioli, G. B., Santos, J. E., Carcione, J. M., & Gei, D. (2016). A model for CO2 storage and seismic monitoring combining multiphase fluid flow and wave propagation simulators. The Sleipner-field case. *Computational Geosciences*, *21*, 223. https://doi.org/10.1007/s10596-016-9607-y.

Sinha, S., Hardy, R. J., Blois, G., Best, J. L., & Sambrook Smith, G. H. (2017). A numerical investigation into the importance of bed permeability on determining flow structures over river dunes. *Water Resources Research*, *53*, 3067–3086.

Tanikawa, W., & Shimamoto, T. (2006). Klinkenberg effect for gas permeability and its comparison to water permeability for porous sedimentary rocks. *Hydrology and Earth System Sciences Discussions*, *3*, 1315–1338.

Tiab, D., & Donaldson, E. C. (2012). *Petrophysics: theory and practice of measuring reservoir rock and fluid transport properties*. Boston: Gulf Professional Publishing.